Special Issue

Journal of Physical Organic Chemistry

Received: 29 October 2007, Revised: 14 December 2007, Accepted: 17 December 2007, Published online in Wiley InterScience: 16 May 2008

(www.interscience.wiley.com) DOI 10.1002/poc.1326

H_2O_2 activation by heteropolyacids with defect structures: the case of γ-$[(XO_4)W_{10}O_{32}]^{n-}$ (X = Si, Ge, n = 8; X = P, n = 7)†

Andrea Sartorel[a]*, Mauro Carraro[a], Alessandro Bagno[a], Gianfranco Scorrano[a] and Marcella Bonchio[a]*

DFT calculations including relativistic and solvent effects have been carried out for elucidating geometries and energies of tetra-protonated, site-defective, polyoxotungstates with general formula γ-$[(XO_4)W_{10}O_{32}]^{n-}$ (X = Si, Ge, n = 8; X = P, n = 7). Converging spectroscopic and computational evidence point to a unique role played by the lacunary structure, and allow to address the electronic and structural factors dictating the protonation sites and equilibria of these complexes, as well as their impact on H_2O_2 activation. In all cases, the evolution of the four terminal W—O functions, bordering the site defect on the polyoxotungstate surface, towards a bis-aquo, bis-oxo structure is preferred over the formation of four terminal hydroxo ligands. Substitution of these W—OH_2 functions with peroxo ligands and their involvement in the oxygen transfer to an alkene acceptor is also supported by DFT calculations.

Supplementary electronic material for this paper is available in Wiley InterScience at http://www.mrw.interscience.wiley.com/suppmat/0894-3230/suppmat/

Keywords: polyoxometalates; proton transfer; catalytic epoxidation; tungsten; density functional calculations

INTRODUCTION

Metal-catalyzed activation of hydrogen peroxide is a well-recognized strategy towards the invention of novel, environmentally sustainable, methods for selective oxygen transfer to organic substrates. Among metal-mediated protocols using hydrogen peroxide as terminal oxidant, those involving competent W(VI)-peroxides are generally characterized by negligible decomposition pathways, and good to excellent selectivities.[1,2] Moreover, as process intensification issues are emerging top-priorities, the design of tailored multi-metal catalysts is attracting considerable attention together with the urgent need for high efficiency and multifunctionality. In this respect, polyoxotungstate architectures provide a key resource for application in catalysis.[1–5] Indeed, polyoxometalates (POMs) self-assemble in aqueous solution giving rise to discrete, multi-metal-oxide clusters with well-defined atom connectivity and tunable size, symmetry, charge, redox, and acidity properties. For this reason, they offer a unique opportunity to probe structure–activity relationships, surface reactivity, and mechanism at the borderline between molecules and bulk solids. Therefore, the assessment of the catalytic events mediated by POMs is instrumental for designing the active sites of the inorganic framework at the molecular level. At the same time, the outcome of these studies will foster additional insights into the elementary steps and functional requirements of heterogeneous metal-oxide surfaces, widely used and preferred, for industrial-scale catalytic applications. In this light, polyoxotungstates, stable under H_2O_2 excess and displaying persistent structures under oxidation turnovers, retain a fundamental interest.[3–9] Worthy of notice is the catalytic performance of the decatungstosilicate $[\gamma\text{-}SiW_{10}O_{36}]^{8-}$ (**SiW**$_{10}$) and of its hybrid derivatives, showing selectivity up to >99% in the epoxidation of internal and terminal double bonds, and a large substrate scope, both in organic media and/or in ionic liquids.[6–11] The catalyst structure features a site defect, whereby a formal loss of two W=O units opens a di-vacant, surface lacuna. This tungsten deficiency leaves a nucleophilic tetra-oxygenated site, bordered by four W(VI) atoms, prone to H_2O_2 coordination (Scheme 1).[9,12] Interestingly, the presence of defects and/or dislocations on solid surfaces is also known to play a major role for the activation of small molecules, but the generally ill-defined nature of the bulk material poses a formidable challenge in the final elucidation of the catalytic mechanism.[13] Therefore, the structural and electronic properties of "lacunary" POMs have been the subject of recent studies addressing their solution speciation and evolution under catalytic regime.[12] In particular the combined use of spectroscopic and computational techniques has proved to be a rewarding strategy to address single- and multiple-proton transfer events on the polyoxometalate surface and their impact on the structural and reactivity properties of the complex.[12,14] Both the basicity of the POM oxygens and the related protonation/deprotonation constants

* *ITM-CNR and Department of Chemical Sciences University of Padova, via Marzolo 1, 35131, Padova, Italy. E-mail: a.sartorel@itm.cnr.it and marcella.bonchio@unipd.it*

a *A. Sartorel, M. Carraro, A. Bagno, G. Scorrano, M. Bonchio ITM-CNR and Department of Chemical Sciences University of Padova, via Marzolo 1, 35131, Padova, Italy*

† *Presented at the 11th European Symposium on Organic Reactivity (ESOR XI), 1–6 July 2007, Faro, Portugal.*

Journal of Physical Organic Chemistry

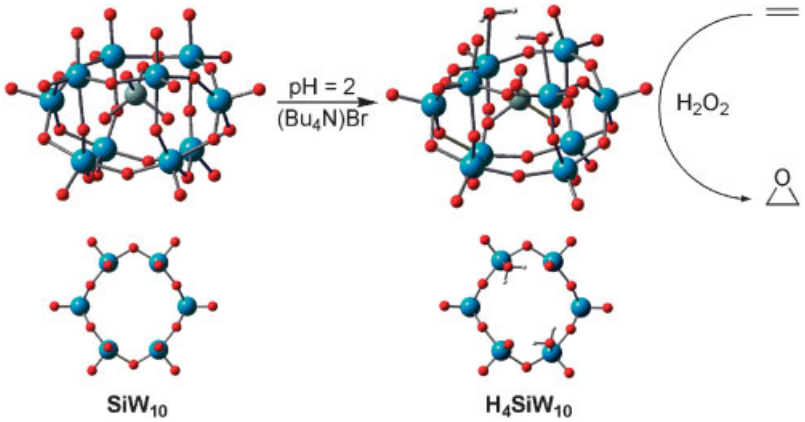

Scheme 1. Optimized structure of γ-$[(SiO_4)W_{10}O_{32}]^{8-}$ (**SiW**$_{10}$) and of the catalytically active tetra-protonated form γ-$[(SiO_4)W_{10}O_{30}(H_2O)_2]^{4-}$ (**H$_4$SiW**$_{10}$); top-view of the di-vacant site defect highlights the on-surface localization of two water molecules. Blue atoms: tungstens; grey atom: silicon; red atoms: oxygens; white atoms: hydrogens.

(thermodynamic effects), together with intramolecular hydrogen-bonding and proton transfer dynamics (kinetic effects) are expected to control the formation of competent peroxo-tungsten functions, responsible for H_2O_2 activation. These arguments have been highlighted by observation of peak epoxidation rates upon tetra-protonation of the polyoxometalate-based catalyst, γ-$[(SiO_4)W_{10}O_{30}(H_2O)_2]^{4-}$ (**H$_4$SiW**$_{10}$), and by assignment of the proton distribution on the inorganic surface, showing the regioselective double-protonation of only two oxo groups, with localization of two coordinated water molecules on the POM lacuna.[12] We report herein a computational investigation extending this outlook within the isostructural POM series of general formula, γ-$[(XO_4)W_{10}O_{32}]^{n-}$ (X = Si, Ge, $n = 8$; X = P, $n = 7$).[15–17] Our approach takes into consideration the evolution of the catalyst, via H_2O_2 coordination, fostering the regioselective peroxidation of the POM lacunary site.[18] Finally, a Frontier Orbital analysis is reported to address the interaction between the competent metal-peroxo groups and a model alkene acceptor, along the oxygen transfer pathway.

EXPERIMENTAL

Computational resources and assistance were provided by the Laboratorio Interdipartimentale di Chimica Computazionale (LICC) at the Department of Chemical Sciences of the University of Padova. Relativistic DFT calculations have been carried out using the Amsterdam density functional (ADF) code,[19] in which all-electron Slater basis sets are available for all atoms of interest. Scalar relativistic effects were taken into account by means of the two-component zero-order regular approximation (ZORA) method,[20–23] adopting the Becke 88 exchange plus the Perdew 86 correlation (BP) functional.[24,25] The basis sets in this work were of triple-zeta quality, singly polarized (TZP), specially optimized for ZORA calculations. Geometries were optimized taking full advantage of molecular symmetry. The solvent effect was modeled by means of the ADF implementation[26] of the COSMO method.[27–29] This method requires a prior definition of atomic radii, which were set (in Å) either at their recommended values (H: 1.3500; O: 1.5167; P: 1.8500; Si: 1.9083; Ge: 2.0333; W: 1.9917). In addition to the dielectric permittivity ε, the solvent is modeled also by an empirical parameterization of non-electrostatic solvation terms derived from the solvation of alkanes.[26,30] Since these parameters are currently available only for water, energies, and gradients can be reliably calculated only for this solvent.[31] Therefore, all calculations assumed water as solvent.

^{183}W NMR spectra were collected at 9.4 T (16.67 MHz) on a Bruker Avance DRX 400 instrument, equipped with a standard (^{31}P–^{109}Ag) 10-mm broadband probe, which could be tuned below its specifications; the $\pi/2$ pulse duration was 50 μs. Chemical shifts are externally referenced to 2 M aqueous Na_2WO_4; typically 10^3 transients were collected in 32 K data points. ^{1}H NMR spectra were obtained at 7.05 T (300.13 MHz) on a Bruker Avance DRX instrument.

Polyoxometalates were prepared according to literature procedures.[6,15]

RESULTS AND DISCUSSION

The active catalyst, **H$_4$SiW**$_{10}$, is isolated at pH = 2 as tetraalkylammonium salt. In agreement with the X-ray evidence, DFT calculations indicate that protonation occurs preferentially on the POM site defect, where the four lacunary oxygens can accommodate a favorable, intramolecular, hydrogen bonding interaction (Scheme 1).[12]

Furthermore, the solution speciation of the title catalyst and possible protonation-dependent structural/dynamic effects have been addressed by NMR spectroscopy. In particular, nuclear magnetic resonance spectroscopy of the ^{183}W nucleus ($I = 1/2$, 14% natural abundance) is an essential tool for the characterization of polyoxotungstates as it provides direct information on the POM framework and symmetry. In aqueous solution, the fully deprotonated **SiW**$_{10}$ anion exhibits a three-line (4:4:2) ^{183}W spectrum, with signals respectively at −98.5, −139.5, and −160.0 ppm, consistent with C_{2v} symmetry (Fig. 1a).[15,32,33] As a consequence of tetra-protonation, the active catalyst, **H$_4$SiW**$_{10}$, displays a solid-state and solution structure with C_2 symmetry. Indeed, the ^{183}W NMR spectrum of **H$_4$SiW**$_{10}$ exhibits five lines with equal intensity, at −94.6, −98.1, −115.6, −118.1, and −193.8 ppm, compatible with the bis(aquo)–bis(oxo) structure, predicted by DFT calculations (Fig. 1b and Scheme 1). Moreover, the observation of a C_2 solution structure implies a slow proton-exchange regime.[12] This phenomenon is also confirmed

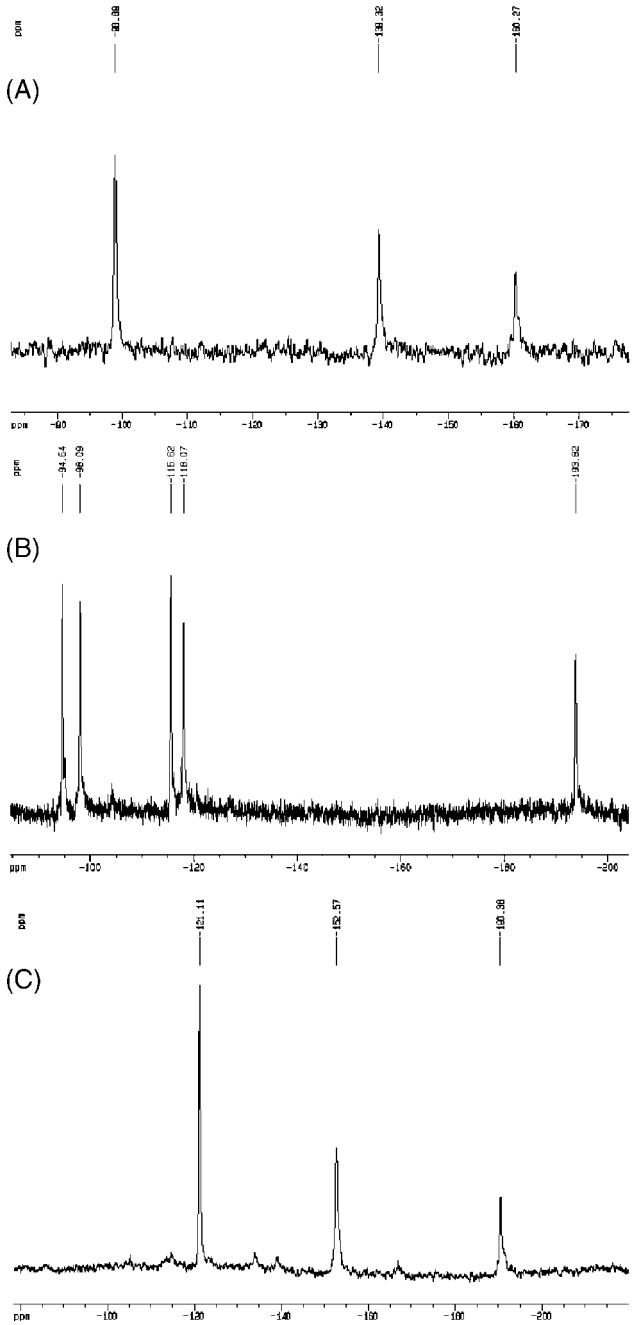

Figure 1. ^{183}W-NMR spectra of: (a) fully deprotonated **SiW**$_{10}$ in D_2O, (b) **H**$_4$**SiW**$_{10}$ in d_6-DMSO, and (c) **H**$_2$**SiW**$_{10}$ formed *in situ* by addition of two equivalents of $(Bu_4N)OH$ to **H**$_4$**SiW**$_{10}$, in d_6-DMSO

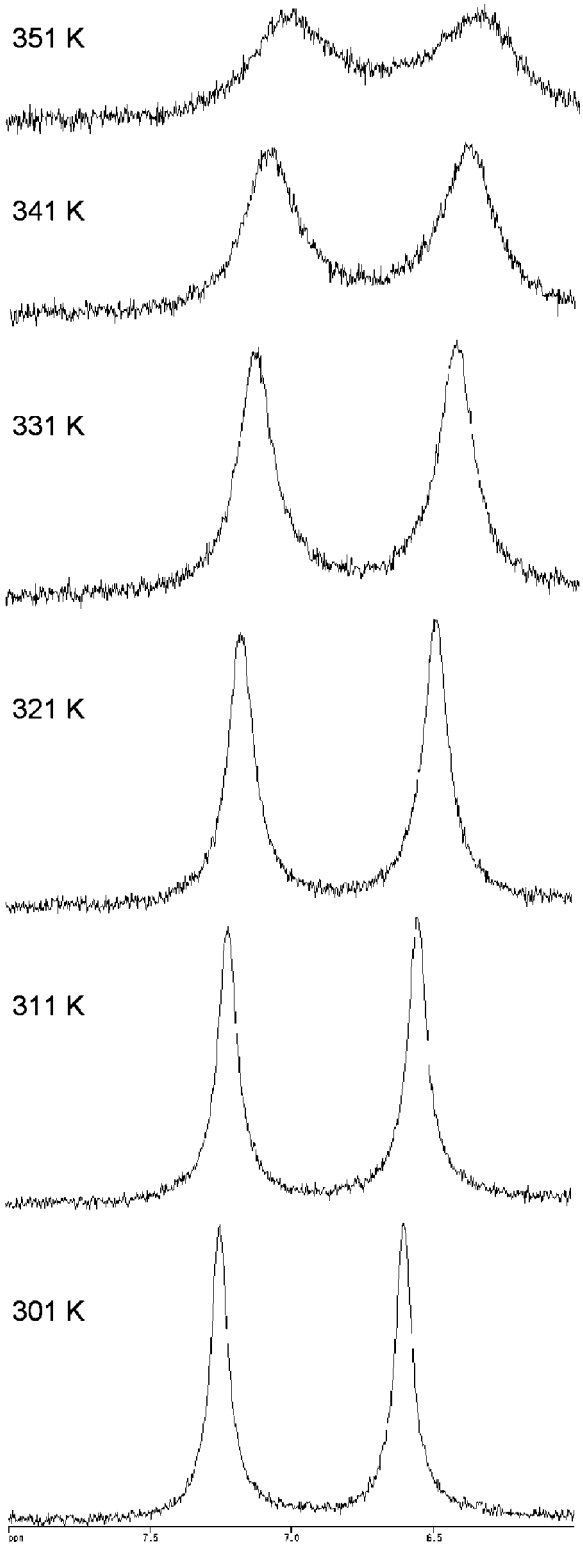

Figure 2. ^{1}H-NMR (6–8 ppm region) of H$_4$-**1** in d_6-DMSO at 301–351 K

by ^{1}H-NMR where two broad 1:1 signals are found at 7.25 and 6.61 ppm, ascribable to two hydrogen types, (Fig. 2).[12] Significantly, the spin system is not modified upon addition of water (10% in d_6-DMSO), and only a modest line-broadening is induced by increasing the temperature up to 351 K (Fig. 2).

The C_{2v} solution structure and fast proton exchange regime are restored upon titration of **H**$_4$**SiW**$_{10}$ with two equivalents of $(nBu_4N)OH$. Converging lines of evidence point to the *in situ* formation of **H**$_2$**SiW**$_{10}$ upon removal of the two more acidic protons within the system, i.e., those not involved in hydrogen bonds. In fact, the ^{1}H-NMR spectrum shows the disappearance of one resonance, while a broad signal at 6.45 ppm is retained, ascribable to the residual two protons involved in H-bonds.[12] Moreover, the corresponding ^{183}W NMR spectrum is composed of three signals with relative intensity 4:4:2, at −121.1, −152.6, and

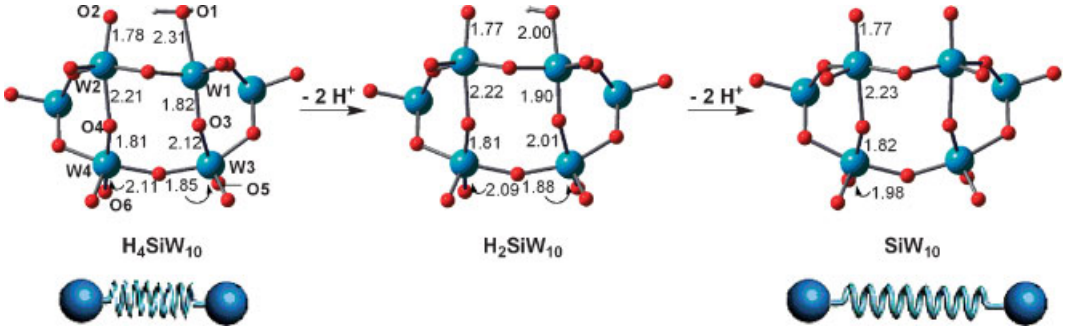

Scheme 2. Calculated structural response of $\mathbf{H_4SiW_{10}}$ upon protonation/deprotonation of the lacunary site (frontal perspective), showing the alternate sequence of long and short *trans* O–W–O bond lengths along the POM skeleton.

−190.4 ppm, respectively, consistent with a pseudo C_{2v} symmetry, implying that at this stage the two protons are in rapid exchange between the two couples of vicinal lacunary oxygens (Fig. 1c and Scheme 2).

The switch to a fast proton exchange regime observed upon deprotonation of $\mathbf{H_4SiW_{10}}$ is likely associated to the release of the "Pfeiffer" compression of the polyoxotungstate structure, induced by the non-symmetric protonation of alternate WO_6 octahedra.[34–36] This effect results in an alternate sequence of long and short *trans* O—W—O bond lengths, along the POM backbone, as can be traced in the bond series O1—W1—O3—W3—O5 and O2—W2—O4—W4—O6, both from computational results and experimental determination (Scheme 2 and Table 1). The chained *trans*-push-pull bond perturbation along the POM skeleton is acting cooperatively to reinforce or suppress the HB donor/acceptor properties of lacunary W—O sites. Indeed, inspection of the optimized geometries of $\mathbf{H_4SiW_{10}}$, $\mathbf{H_2SiW_{10}}$, and $\mathbf{SiW_{10}}$, (Scheme 2) shows a substantial variation of the distance between two adjacent oxygen sites in the lacunary pocket (O1 and O2 in Scheme 2), which increases upon deprotonation in the order 2.675< 2.954< 3.343 Å. This evidence speaks in favor of a stronger hydrogen bonding interaction involving the protonated W—O functions in $\mathbf{H_4SiW_{10}}$ with respect to $\mathbf{H_2SiW_{10}}$. Therefore, a spring-like behavior can be envisaged, whereby the POM framework undergoes a chemically stimulated physical response, with compression upon protonation, and relaxation upon deprotonation (Scheme 2). The major potential associated to this property is the tuning of structural/electronic features and mechanistic effects, possibly induced by multiple proton transfer on extended inorganic surfaces.

Taken as a whole, in the case of the $\mathbf{H_4SiW_{10}}$ heteropolyacid, the combined X-ray, DFT calculations and heteronuclear NMR evidence indicates a preferential regioselective distribution of the four protons over only two lacunary oxygen, thus leading to a bis(aquo)–bis(oxo) isomer rather than promoting the mono-protonation of all oxygen sites with the formation of four terminal hydroxo ligands. Indeed the structure stabilization induced by the "Pfeiffer compression" for the hypothetical tetra-hydroxo isomer appears to be negligible.

DFT calculations support an analogous proton distribution for other isostructural polyoxotungstates, thus pointing to a general behavior associated to hetoropolyacids with site defects of formula γ-$[(XO_4)W_{10}O_{32}]^{n-}$ (X = Si, Ge, $n = 8$; X = P, $n = 7$). The stabilization energies of $\mathbf{H_4XW_{10}}$, with X = Si, Ge, P, as bis*(*aquo)–bis*(*oxo) isomer with respect to the tetra-hydroxo formulation are reported in Table 1, and range between 2.0 and 4.6 kcal mol^{-1}. Moreover, their W—O distances along the polyoxometalate skeleton are in fair agreement with the experimental ones observed for $\mathbf{H_4SiW_{10}}$,[6] with differences between consecutive W—O bonds up to 0.4 Å, and a minor

Table 1. Stabilization energies of $\mathbf{H_4SiW_{10}}$, $\mathbf{H_4GeW_{10}}$, and $\mathbf{H_4PW_{10}}$ respect to the relative tetra-hydroxo isomers, and relevant geometric parameters of the optimized and experimental structures

Parameter	$\mathbf{H_4SiW_{10}}$	$\mathbf{H_4SiW_{10}}$, exp[6]	$\mathbf{H_4GeW_{10}}$	$\mathbf{H_4PW_{10}}$	$\mathbf{H_2SiW_{10}}$
ΔE (kcal mol^{-1})[a]	4.60	—	3.19	2.06	—
O1–W1 (Å)	2.31	2.16	2.33	2.25	2.00
W1–O3 (Å)	1.82	1.82	1.81	1.83	1.90
O3–W3 (Å)	2.12	2.05	2.14	2.08	2.01
W3–O5 (Å)	1.85	1.85	1.85	1.86	1.88
O6–W4 (Å)	2.11	2.08	2.13	2.07	2.09
W4–O4 (Å)	1.81	1.79	1.81	1.82	1.81
O4–W2 (Å)	2.21	2.20	2.22	2.15	2.22
W2–O2 (Å)	1.78	1.72	1.78	1.78	1.77

[a] Calculated with respect to the hypothetical tetra-hydroxo isomer.

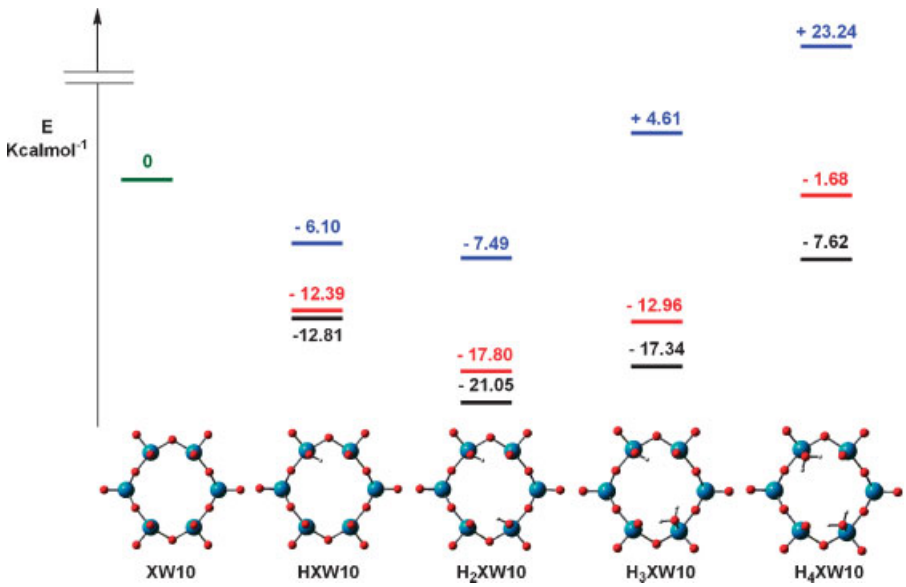

Figure 3. Calculated energies associated to the four sequential protonation of the lacunary site of $\mathbf{XW}_{10}$, with X = Si (black lines), Ge (red lines), and P (blue lines)

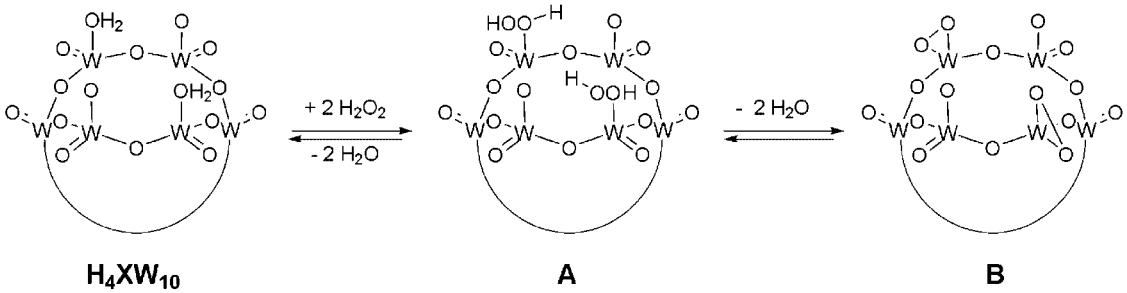

Scheme 3. Peroxidation of the POM surface by ligand exchange on the lacunary site, fostered by localization of two water molecules

influence of the central heteroatom and of the overall polyanionic charge.

Inspection of the calculated relative energies along the stepwise protonation pathway from $\mathbf{XW}_{10}$ to $\mathbf{H_4XW}_{10}$, X = Si, Ge, P, (Fig. 3), support the presence of two types of protons whose different acidity is dictated by intramolecular hydrogen bonding.

The protonation sites and equilibria of the heteropolyacids are expected to affect their catalytic performance. In the epoxidation of *cis*-cyclooctene catalyzed by $\mathbf{H_4SiW}_{10}$, the turnover frequency (TOF) drops linearly upon addition of two equivalents of (nBu$_4$N)OH, then levels off to a plateau value upon further addition of base (TOF = 112, 67, 28, 17, and 16 h^{-1} upon titration of $\mathbf{H_4SiW}_{10}$ with 0, 1, 2, 3, and 4 equivalents of (nBu$_4$N)OH).[12] This result points out the major role played only by two, out of four, acidic protons on the POM surface, in promoting oxygen transfer. Therefore, fast catalysis from $\mathbf{H_4SiW}_{10}$ is likely prompted by the two W—OH_2 functions bordering the POM lacuna. Indeed the regioselective double protonation of two, out of four, lacunary tungsten sites, results in the formation of two incipient leaving groups, thus fostering ligand exchange within the coordination sphere of each independent catalytic site and their peroxidation in the presence of H_2O_2 excess (Scheme 3). Replacement of water molecules with peroxo-ligands has been recently supported by Cryospray mass spectrometry (CSI-MS), and by ^{183}W-NMR evidence.[9]

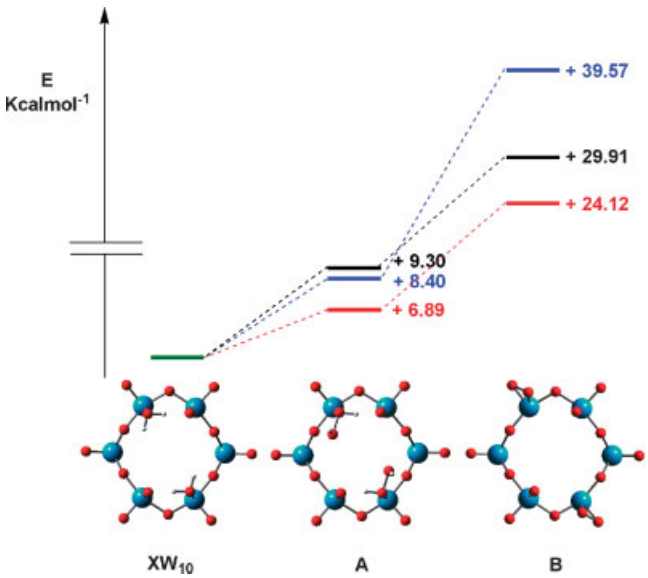

Figure 4. Calculated energies of bis-η^1-hydroperoxo (**A**) and *bis*-η^2-peroxo (**B**) intermediates formed upon water substitution from the parent bis(aquo)–bis(oxo) structure of $\mathbf{XW}_{10}$, X = Si (black lines), Ge (red lines), and P (blue lines)

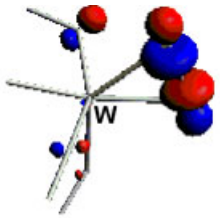

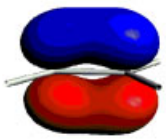

X	E (σ* O-O), a.u.
Si	- 0.0684
Ge	- 0.0828
P	- 0.0970

peroxide LUMO (σ* O-O) alkene HOMO (π C-C)

Figure 5. Representation and energies of the peroxide LUMO (σ^*_{O-O}) of the bis-η^2-peroxo, bis(oxo) **B** complexes, and ethylene HOMO (π_{C-C})

Interestingly, the computed energies associated to the loss of a water ligand are +13.3, +10.8, and +18.3 kcal mol^{-1} for $\mathbf{H_4SiW_{10}}$, $\mathbf{H_4GeW_{10}}$, and $\mathbf{H_4PW_{10}}$, respectively, and thus indicate that coordinated water is more labile in $\mathbf{H_4GeW_{10}}$, which is then expected to be even more prone to peroxidation than $\mathbf{H_4SiW_{10}}$. A computational study has also been performed to gain additional insights into the stepwise evolution of the competent catalyst under turnover regime. Geometries and energies of postulated bis-η^1-hydroperoxo (**A**) and bis-η^2-peroxo (**B**) intermediates formed upon water substitution from the parent bis(aquo)–bis(oxo) structure, have been calculated for the diverse POMs under examination (Fig. 4). In all cases, the calculated bond lengths for the O—O functions are in the range 1.469–1.507 Å, thus showing a good agreement with the experimental determination available for related d^0 metal peroxides.[37] Notably, whereas the formation of the bis-η^2-peroxide is always endothermic, it is least unfavorable in the case of the germanium derivative, with an energy gain of 5.8 and 15.4 kcal mol^{-1} with respect to the silicon and phosphorous analogues, respectively (Fig. 4).

Oxygen transfer by d^0 transition metal peroxo species generally involves an electrophilic attack of the peroxo function on the electron-rich substrate.[38] The frontier orbital interaction between the olefin HOMO ($\pi_{C—C}$) and the peroxide LUMO ($\sigma^*_{O—O}$) is outlined in Fig. 5 for the three species under investigation.[39] The computed energies of these latter are influenced by the nature of the central heteroatom in the POM structure. In particular, the LUMOs of the $\mathbf{PW_{10}}$ and $\mathbf{GeW_{10}}$ η^2-peroxocomplexes, lie at a lower energy with respect to the corresponding orbital of the $\mathbf{SiW_{10}}$ derivative, by 17.9 and 9.0 kcal mol^{-1}, respectively, thus yielding a more favorable interaction with the alkene HOMO (Fig. 5).

A reactivity change is then expected in the series of isostructural complexes. Considering both the peroxidation step and the oxygen transfer properties, computations are actually drawing attention towards both the $\mathbf{H_4GeW_{10}}$ and $\mathbf{H_4PW_{10}}$ species as promising epoxidation catalysts, for which an outstanding performance, even superior to $\mathbf{H_4SiW_{10}}$, can be predicted. Further efforts will then be directed to the optimization of the procedure for their synthesis.

Acknowledgements

Financial support from CNR, MIUR (FIRB CAMERE-RBNE03JCR5; PRIN contract No. 2006034372), ESF COST D29 and D40 actions is gratefully acknowledged.

REFERENCES

[1] J-E Bäckvall, in *Modern Oxidation Methods*, Wiley-VCH, Weinheim, **2004**.
[2] B. S. Lane, K. Burgess, *Chem. Rev.* **2003**, *103*, 2457–2474 .
[3] W. Adam, B. L. Alsters, R. Neumann, C. R. Saha-Möller, D. Sloboda-Rozner, R. Zhang, *J. Org. Chem.* **2003**, *68*, 1721–1728.
[4] D. Sloboda-Rozner, P. L. Alsters, R. Neumann, *J. Am. Chem. Soc.* **2003**, *125*, 5280–5281.
[5] D. Sloboda-Rozner, P. Witte, P. L. Alsters, R. Neumann, *Adv. Synth. Catal.* **2004**, *346*, 339–345.
[6] N. Mizuno, K. Kamata, K. Yonehara, Y. Sumida, *Science.* **2003**, *300*, 964–966.
[7] N. Mizuno, K. Yamaguchi, K. Kamata, *Coord. Chem. Rev.* **2005**, *249*, 1944–1956.
[8] K. Kamata, Y. Nakagawa, K. Yamaguchi, N. Mizuno, *J. Catal.* **2004**, *224*, 224–228.
[9] K. Kamata, M. Kotani, K. Yamaguchi, S. Hikichi, N. Mizuno, *Chem. Eur. J.* **2007**, *13*, 639–648.
[10] M. Carraro, L. Sandei, A. Sartorel, G. Scorrano, M. Bonchio, *Org. Lett.* **2006**, *8*, 3671–3674.
[11] S. Berardi, M. Bonchio, M. Carraro, V. Conte, A. Sartorel, G. Scorrano, *J. Org. Chem.* **2007**, *72*, 8954–8957.
[12] A. Sartorel, M. Carraro, A. Bagno, G. Scorrano, M. Bonchio, *Angew. Chem. Int. Ed.* **2007**, *46*, 3255–3258.
[13] D. H. Wells, A. M. Joshi, W. N. Delgass, K. T. Thomson, *J. Phys. Chem. B* **2006**, *110*, 14627–14639.
[14] X. Fang, C. L. Hill, *Angew. Chem. Int. Ed.* **2007**, *46*, 3877–3880.
[15] J. Canny, A. Tézé, R. Thouvenot, G. Hervé, *Inorg. Chem.* **1986**, *25*, 2114–2119.
[16] N. H. Nsouli, B. S. Bassil, M. H. Dickman, U. Kortz, B. Keita, L. Nadjo, *Inorg. Chem.* **2006**, *45*, 3858–3860.
[17] A. Tézé, G. Hervé, *Inorg. Synth.* **1990**, *27*, 85–96.
[18] J. Server-Carrio, J. Bas-Serra, M. E. Gonzalez-Nunez, A. Garcia-Gastaldi, G. B. Jameson, L. C. W. Baker, R. Acerete, *J. Am. Chem. Soc.* **1999**, *121*, 977–984.
[19] G. te Velde, F. M. Bickelhaupt, E. J. Baerends, C. Fonseca Guerra, S. J. A. van Gisbergen, J. G. Snijders, T. Ziegler, *J. Comput. Chem.* **2001**, *22*, 931–967. See also: ADF 2006.01, ADF User's Guide. http://www.scm.com
[20] S. K. Wolff, T. Ziegler, E. van Lenthe, E. J. Baerends, *J. Chem. Phys.* **1999**, *110*, 7689–7698.
[21] J. Autschbach, in *Calculation of NMR and EPR Parameters*, (Eds.: M. Kaupp, M. Bühl, V. G. Malkin). Wiley-VCH, Weinheim, **2004**. Chapter 14.
[22] E. van Lenthe, E. J. Baerends, J. G. Snijders, *J. Chem. Phys.* **1993**, *99*, 4597–4610.
[23] E. van Lenthe, Ph.D. Thesis, Vrije Universiteit, Amsterdam, **1996**.
[24] A. D. Becke, *Phys. Rev. A* **1988**, *38*, 3098–3100.
[25] J. P. Perdew, *Phys. Rev. B* **1986**, *33*, 8822–8824.
[26] C. C. Pye, T. Ziegler, *Theor. Chem. Acc.* **1999**, *101*, 396–408.
[27] A. Klamt, G. Schüürmann, *J. Chem. Soc., Perkin Trans. 2* **1993**, 799–805.
[28] A. Klamt, V. Jones, *J. Chem. Phys.* **1996**, *105*, 9972–9981.
[29] A. Klamt, *J. Phys. Chem.* **1995**, *99*, 2224–2235.
[30] T. N. Truong, E. V. Stefanovich, *Chem. Phys. Lett.* **1995**, *240*, 253–260.
[31] It is worth noting that the thermodynamics of solvation of hydrocarbons is profoundly different according to whether the solvent is

water or practically any other liquid. See e.g., W. Blokzijl, J. B. F. N. Engberts, *Angew. Chem. Int. Ed. Engl.* **1993**, *32*, 1545–1579.
[32] A. Bagno, M. Bonchio, *Angew. Chem. Int. Ed.* **2005**, *44*, 2023–2026.
[33] A. Bagno, M. Bonchio, J. Autschbach, *Chem. Eur. J.* **2006**, *12*, 8460–8471.
[34] M. T. Pope, *Inorg. Chem.* **1976**, *15*, 2008–2010.
[35] J. F. Garvey, M. T. Pope, *Inorg. Chem.* **1978**, *17*, 1115–1118.
[36] U. Kortz, S. S. Hamzeh, N. A. Nasser, *Chem. Eur. J.* **2003**, *9*, 2945–2952.
[37] G. Strukul: *Catalytic Oxidations with Hydrogen Peroxide as Oxidant*, (Ed.: ,G. Strukul). Kluwer Academic Publishers, Dordrecht, **1992**. The tetra-peroxo complex derived from addition of H_2O_2 to the four lacunary W(VI) of β_3-$[Co^{II}W_{11}O_{39}]^{10-}$ has been characterized by X-ray analysis and found to be reactive in the epoxidation of 2-cyclohexenol, see reference [18].
[38] F. E. Kühn, A. M. Santos, R. W. Rocksy, E. Herdweck, W. Scherer, P. Gisdakis, I. V. Yudanov, C. Di Valentin, N. Rösch, *Chem. Eur. J.* **1999**, *5*, 3603–3615 and references therein.
[39] The σ^* LUMO delocalized on the peroxide moiety is the LUMO+19, LUMO+16, and LUMO+16 for the Si, Ge, and P derivatives, respectively. The interaction between the peroxide HOMO and the alkene LUMO is less important and was not considered.